# Strong coupling between the spin polarization of Mn and Tb in multiferroic $TbMnO_3$ determined by x-ray resonance exchange scattering

J. Voigt,[1] J. Persson,[1] J. W. Kim,[2] G. Bihlmayer,[1] and Th. Brückel[1]
[1]*Institut für Festkörperforschung, Forschungszentrum Jülich, 52425 Jülich, Germany*
[2]*Ames Laboratory, Ames, Iowa 50011, USA*
(Received 14 August 2007; published 25 September 2007)

We report on an x-ray resonance exchange scattering (XRES) study of multiferroic $TbMnO_3$. Magnetic scattering is observed close to the Mn $K$ edge and the Tb $L_{III}$ and $L_{II}$ edges. Surprisingly, Tb shows XRES also in the paraelectric phase, where neutron diffraction results suggested the $4f$ moments to be disordered. The temperature dependence of the XRES intensities shows a distinct kink close to the ferroelectric transition temperature $T_C$ for all absorption edges. We were able to model the temperature dependence for all edges, assuming a strong coupling of Mn and Tb magnetism via the spin polarized $5d$ conduction band. We argue that the hybridization between Mn and Tb states is a prerequisite for the multiferroic effect in this material.

DOI: 10.1103/PhysRevB.76.104431 PACS number(s): 75.47.Lx, 75.25.+z, 78.70.Ck

## I. INTRODUCTION

"The revival of the magnetoelectric effect"[1] was triggered strongly by the observation of multiferroic behavior in a variety of manganites containing small rare earth cations.[2–4] A strong coupling exists in these compounds between the ferroelectric polarization and an (anti)ferromagnetic order of the spin system. From the theoretical point of view, they challenge the usual explanation for ferroelectricity and magnetic order in transition metal systems. The former usually requires the $d^0$-ness, i.e., empty $d$ orbitals, while the latter can only appear if partly filled $3d$ orbitals are present. From the applications point of view, the control of electrical degrees of freedom via magnetic fields and vice versa offers fascinating new perspectives, e.g., devices, where a magnetic field changes the optical properties.

$TbMnO_3$ crystallizes in the perovskite structure. Hereafter, we use the space group setting *Pbnm* to index the reflections. The magnetic structure of $TbMnO_3$ has been studied by several groups using neutron diffraction.[5–7] At the Néel temperature $T_N$=41 K, an incommensurate magnetic structure appears with a propagation vector $\boldsymbol{Q}=(0\ q_m\ 0)$, $q_m \approx 0.29$ r.l.u. The modulation is mainly sinusoidal, and the moments are aligned along the $b$ direction. At the ferroelectric transition temperature $T_C$=28 K, the magnetic structures become spiral, with the ordered moment mainly in the $bc$ plane.[7] The authors attribute a small $a$-axis component to the $Tb^{3+}$ ions. Below this temperature, the propagation vector varies only slightly with temperature. The broken inversion symmetry due to the noncollinear magnetic structure provides a mechanism for the formation of a ferroelectric polarization along the $c$ direction.[8–10] Microscopically, it has been explained as an inverse Dzyaloshinskii-Moriya interaction. Below 8 K, the $Tb^{3+}$ subsystem orders with $q_{m,Tb}$=0.42 r.l.u.

In this paper, we show with element and band specific x-ray resonance exchange scattering (XRES) that the spin polarizations of Mn and Tb are more intimately connected with each other than the neutron data suggested. We argue that this consists an important ingredient for the appearance of ferroelectricity in $TbMnO_3$.

## II. EXPERIMENT

A single crystal was grown by the floating zone method. Specific heat measurements gave similar results as published by Kimura *et al.*,[2] with $T_N$=41 K and $T_C$=26 K (maximum of the lambda anomaly). The crystal with polished (010) surface was mounted into a closed cycle cryostat at the beamline 6-ID-B of the Advanced Photon Source in Argonne. Rocking curves of the (041) reflection revealed a good sample quality with a mosaic spread of less than 0.05°. The temperature was varied between 7 and 70 K. To assure a good thermal contact, the sample chamber was filled with He exchange gas. For polarization analysis, we used the (006) reflection of a pyrolytic graphite crystal at both Tb absorption edges. At the Mn $K$ edge, we employed a Cu (220) crystal. The scattering plane was chosen vertically, hence the incoming light was $\sigma$ polarized to more than 99.5%. The analyzer suppressed the $\sigma'$ polarization typically by a factor larger than 100. Since charge scattering does not change the polarization, the $\sigma \rightarrow \pi'$ geometry is mainly sensitive to magnetic scattering.[11,12] The temperature dependence of the magnetoelastic lattice modulation $q_l$ was measured using the (002) reflection of the pyrolytic graphite analyzer, detecting both $\sigma'$ and $\pi'$ polarized photons. To probe the temperature dependence of the magnetic propagation vector $q_m$, we performed linear scans in reciprocal space along the $[0k1]$ direction. The temperature dependence of the $b$ lattice constant was determined from the (020) and (040) reflections. For the energy dependence, we fixed the scattering vector at $\boldsymbol{Q}=(0\ 4-q_m\ 1)$ for the respective temperature and varied the incoming photon energy. Additionally, we probed the $[0k0]$ direction at low temperature. These reflections correspond to a magnetic structure denoted $C$ type and $F$ type by Kajimoto *et al.*[6] using the Wollan-Koehler scheme.[13] Rotating the sample around these scattering vectors, we obtain the orientation of the contributing magnetic moments. To account for the different geometrical conditions as the sample is rotated, the data are normalized to the integrated intensity of the (040) Bragg reflection.

## III. RESULTS

Performing linear scans in reciprocal space along the $(0k1)$ direction, we observed the magnetoelastic lattice

 

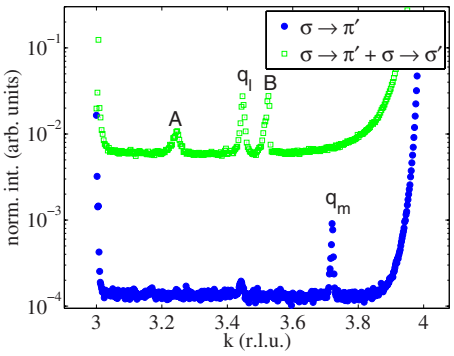


FIG. 1. (Color online) Linear $\boldsymbol{Q}$ scans along $(0k1)$ normalized to monitor counts. The data without polarization analysis were taken at an energy $E=7.5$ keV and $T=32$ K. The $\sigma \rightarrow \pi'$ data were taken at the maximum of the Tb $L_{\mathrm{III}}$ resonance (see Fig. 2), $E=7.518$ keV and $T=7$ K. The peaks denoted with A and B are background features.

modulation without polarization analysis ($k=q_l$) and the magnetic modulation $k=q_m$ in $\sigma \rightarrow \pi'$ geometry (Fig. 1). The widths of the peaks (full width at half maximum) are 0.008 and 0.005 r.l.u. for the lattice modulation and the magnetic peak, respectively. This is well above the instrumental resolution, which can be estimated from the width of the (041) Bragg reflection in a reciprocal lattice scan. Allowing for the instrumental resolution of 0.002 r.l.u., we deduce coherence lengths parallel to the [010] direction of 750(20) and 1250(60) Å, respectively.

The resonant nature of the $q_m$ peak is clear from the energy dependence shown in Fig. 2. Magnetic resonant scattering is observed at the Mn $K$ edge and at the Tb $L_{\mathrm{III}}$ and $L_{\mathrm{II}}$ absorption edges. The magnetic origin of the signal is confirmed by the $\sigma \rightarrow \pi'$ geometry.[12] The strength of the resonance depends usually on the overlap between the involved orbitals. In an ionic picture, the resonant scattering process at

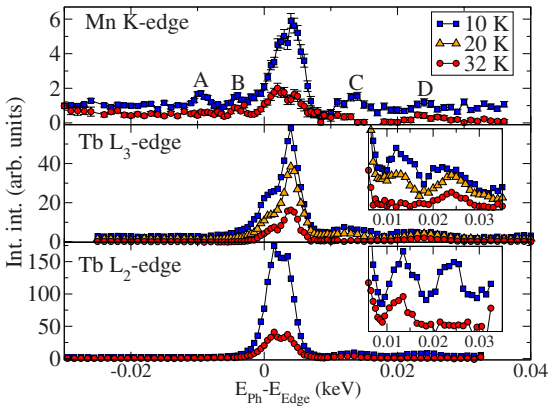


FIG. 2. (Color online) Energy dependence of the peak intensity $(0\ 4-q_m\ 1)$ for the different absorption edges at different temperatures. The data are corrected for absorption. The zero of the energy scale is given by the point of inflection from the fluorescence at the different absorption edges, respectively (not shown): $E_{\mathrm{Mn},K}=6.549$ keV, $E_{\mathrm{Tb},L_{\mathrm{III}}}=7.515$ keV, and $E_{\mathrm{Tb},L_{\mathrm{II}}}=8.253$ keV. The insets show the energy range $0.006<E_{\mathrm{Ph}}-E_{edge}<0.035$ keV on a reduced scale.

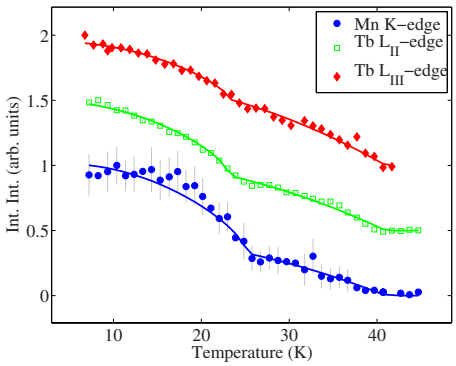


FIG. 3. (Color online) Temperature dependence of the XRES at the different absorption edges. The solid lines are refinements to the data using a molecular field model. The data were normalized to the maximum values of each set and offset for clarity.

the Mn $K$ edge would involve virtual transitions of Mn $1s$ electrons to $4p$ states, with a subsequent decay into $1s$ states for electrical dipole transitions. At the Tb $L_{\mathrm{III}}$ and $L_{\mathrm{II}}$ edges, electrical dipole transitions from the $2p$ level into $5d$ states occur. The strength of the resonance is clearly stronger at the Tb absorption edges. This is expected, since the overlap between $2p$ and $5d$ states is larger than the overlap between $1s$ and $4p$ states. However, a resonance enhancement of 6, as we observed at the Mn absorption edge, is rather strong for magnetic transition metals, e.g., Ref. 14. We observed similar features (A–D in Fig. 2) at the different edges with respect to the edge position. The preedge features at the Mn edge may be attributed to quadrupole transitions into intermediate $3d$ states. These intermediate states are lowered in energy due to the reduced screening of the core hole.

It is intriguing that feature C vanishes at the Tb $L_{\mathrm{III}}$ edge in the paraelectric phase, while feature D disappears at the Tb $L_{\mathrm{II}}$ edge. To determine the edge position, we measured the fluorescence yield across the absorption edges and deduced the point of inflection: $E_{\mathrm{Mn},K}=6.549$ keV, $E_{\mathrm{Tb},L_{\mathrm{III}}}=7.515$ keV, and $E_{\mathrm{Tb},L_{\mathrm{II}}}=8.253$ keV.

The XRES vanishes at all three edges at about 41 K. Close to the phase transition at $T_C \approx 26$ K, the integrated intensity shows a kink for the different absorption edges (see Fig. 3). While the error bars at the Mn edge are rather large, the intensity saturates faster at the Mn edge. This could reflect the different Brillouin functions for the $Tb^{3+}$ ions ($J=6$) as compared to the $Mn^{3+}$ ions ($S=2$). Following the temperature dependence of the propagation vector, we observed a clear thermal hysteresis in the magnetically ordered paraelectric state (Fig. 4), both in the magnetic modulation and in the lattice modulation. We did not close the first hysteresis loop in the paramagnetic state. Later on, we recorded a second hysteresis loop up to 50 K. Below 25 K, the different hysteresis loops cannot be distinguished. The thermal hysteresis is not present for the scattered intensities, neither from the lattice modulation nor from the magnetic structure.

The azimuthal dependence, shown in Fig. 5, is proportional to $\cos^2(\Psi+\Psi_0)$, $\Psi$ denoting the azimuthal angle. The angle $\Psi$ is measured with respect to the [100] direction. The $(0\ 3+q_m\ 0)$ ($C$ type) intensity vanishes completely for $\Psi \approx 90°$. In contrast, the peak $(0\ 4-q_m\ 0)$, which is $F$ type, is

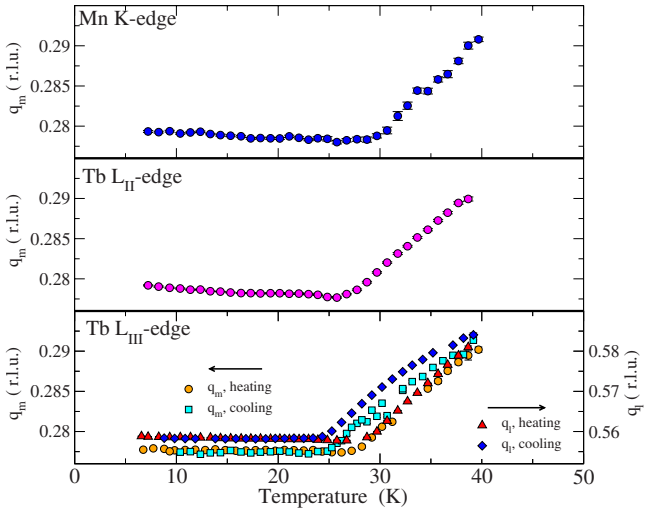


FIG. 4. (Color online) Temperature dependence of the magnetic and lattice modulation vectors at the different edges. The data are corrected for the temperature dependence of the $b$ lattice constant.

well above the background level at $\Psi \approx 0°$. The difference in $\Psi_0$ is very close to 90°. The azimuthal dependence provides further insight into the magnetic structure of $TbMnO_3$. For electrical dipole transitions $E_1$ from an initial polarization $\boldsymbol{\epsilon}$ to a final polarization $\boldsymbol{\epsilon}'$, the resonant scattering amplitude for the $n$th ion with a magnetic moment in the direction of the unit vector $\hat{z_n}$ can be written as[12]

$$f_{nE_1}^{XRES} = (\hat{\boldsymbol{\epsilon}}' \cdot \hat{\boldsymbol{\epsilon}})F^{(0)} - i(\hat{\boldsymbol{\epsilon}}' \times \hat{\boldsymbol{\epsilon}}) \cdot \hat{z_n} F^{(1)} + (\hat{\boldsymbol{\epsilon}}' \cdot \hat{z_n})(\hat{\boldsymbol{\epsilon}} \cdot \hat{z_n})F^{(2)}. \tag{1}$$

The $F^{(0,1,2)}$ denote the oscillator strength. The first term contributes to charge scattering. The last term produces second harmonic reflections as it is quadratic in the magnetic moment. Hence, we have to investigate only the second term for the reflection under consideration. For the chosen $\sigma \rightarrow \pi'$ scattering geometry, the intensity is then proportional to the scalar product $|\hat{\boldsymbol{k}_f} \cdot \hat{z_n}|^2$, i.e., the projection of the magnetic moment onto the direction of the outgoing wave vector. For a finite $b$ component of the magnetic moment, the projection onto $\boldsymbol{k}_f$ never vanishes. The $(0\ 3+q_m\ 0)$ intensity reaches maximum when the scattering plane contains the [100] direction. If it is perpendicular to the scattering direction, the reflection cannot be distinguished from the background. Hence, we observed the spin polarization of the $5d$ states along the [100] direction at the $(0\ 3+q_m\ 0)$ reflection, in accordance with the neutron results.[7] In contrast, the azimuthal scans at the $(0\ 4-q_m\ 0)$ reflection show a phase shift of 90° as compared to the $(0\ 3+q_m\ 0)$ peak, indicating that the spin polarization along the [001] direction contributes to the $(0\ 4-q_m\ 0)$ reflection.

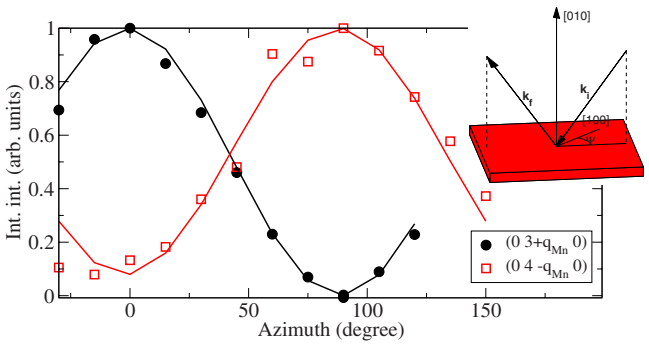


FIG. 5. (Color online) Azimuthal dependence for the $(0\ 3+q_m\ 0)$ ($C$ type) and $(0\ 4-q_m\ 0)$ ($F$ type) reflections. The integrated intensity was obtained from rocking curves across the reflections and normalized to the integrated intensity of the (040) Bragg peak. The azimuthal scan was performed at base temperature $T \approx 6$ K and $E = 8.255$ keV. The inset illustrates the scattering geometry and the definition of $\Psi$. $\Psi$ is measured with respect to the reference direction [100].

## IV. DISCUSSION

The most surprising result of the present study is the observation of element specific XRES in Tb in the paraelectric phase, i.e., in the collinear magnetic phase. According to the neutron diffraction results, the Tb sublattice does not contribute to the magnetic scattering.[7] A recent XRES study on $DyMnO_3$ reports also on an induced Dy moment in the ferroelectric state, but not in the paraelectric state.[18] To understand this, we consider the resonant scattering process in more detail. As mentioned above, the virtual transitions involve mainly the $5d$ states of the rare earth (RE) elements as intermediate states. Hence, one measures the spin polarization of the $5d$ states. The double peak resonance can be explained by a splitting of the $5d$ states in the ordered state. Similar structures are also found in bulk Tb.[15,16] For a metal, the band splitting could be induced by the magnetic order of the transition metal sublattice as found in $DyFe_4Al_8$.[17] To test this assumption, we analyzed the temperature dependence of the resonant signals by assuming a mean field model. The reduced sublattice magnetization can be written[19] as

$$M = B_J\left[\frac{3J}{(J+1)}\frac{T_N}{T}M\right]. \tag{2}$$

$J$ denotes the total angular momentum. As mentioned before, the shape of the temperature dependence is different at the different edges. In our mean field model, we considered a purely induced Tb moment at elevated temperatures, using $J=S=2$. Below the ferroelectric phase transition, we introduced a further component, with $J=6$ for the Tb absorption edges and an additional $S=2$ component at the Mn edge. If we follow the analysis of Kenzelmann *et al.*, the additional component corresponds to the second irreducible representation that is needed to describe the neutron data at 15 K. To fit the integrated intensities, we assume that the XRES is proportional to the square of the magnetic moment:

$$I = (A_1 M_1 + A_2 M_2)^2. \tag{3}$$

From the analysis, we deduced the Néel temperature of 40.9(2) K, in agreement with the previous results and our specific heat data. For the kink temperature $T_{N'}$, we found a value of 23.2(2) K at both Tb absorption edges, slightly

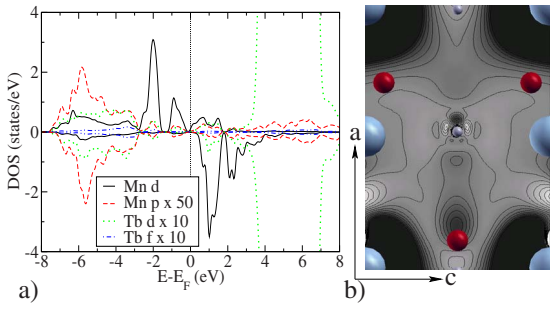


FIG. 6. (Color online) (a) Partial density of states for Mn 3*d* and 4*p* states and Tb 4*f* and 5*d* states from density functional theory, calculated from a model assuming disordered Tb 4*f* moments. The Mn 4*p* and the Tb density of states have been multiplied by a factor 50 and 10 for clarity, respectively. (b) Magnetization density of the first unoccupied Mn peak ($0<E-E_F<2$ eV). Dark gray color represents higher magnetization density. Slice through a Tb atom in a plane normal to the [010] direction. Small gray sphere, Tb; red (dark gray) spheres, O; and big light blue (light gray) spheres, Mn.

lower than the phase transition temperature deduced from the specific heat data. The kink temperature determined from XRES at the Mn *K* edge coincides, within the experimental error, with the transition temperature from the specific heat data.

Particularly, for the Tb edge, the shape of the integrated intensity is well reproduced. This leads us to conclude that the 5*d* spin polarization is induced by Mn in the paraelectric phase. At low temperature, the 4*f* ordering of the $Tb^{3+}$ ions leads to an additional spin polarization in the 5*d* states. The structural information obtained by XRES shows that the magnetism of the Mn and Tb sublattices are intimately connected. While such a spin polarization in the conduction band of a RE ion by the magnetic order of a 3*d* element has been observed earlier in a metal,[17] it is extremely unusual to observe such a strong coupling for an insulating material. The calculation of the local partial density of states in the framework of the density functional theory within the generalized gradient approximation[20] supports our interpretation of the data (see Fig. 6). The model explicitly suppresses the ordering of the Tb 4*f* states.[21] The atomiclike 3*d* states lead to narrow peaks below (above) the Fermi energy in the majority (minority) band. The partial Mn 4*p* and the Tb 5*d* densities of states have maxima at the same energy. Within this model, the similar shapes of the main resonances can be understood. Our simplified model is not intended to account for all observed spectroscopic features. It shows, however, that the magnetization density at the Tb position in this energy range is induced by the neighboring *E*-type ordered Mn [see Fig. 6(b)], giving rise to the XRES in the paraelectric state.

## V. CONCLUSION

In conclusion, we have investigated the XRES from $TbMnO_3$. Just below the Néel temperature we detect a spin polarization in the 5*d* states of Tb. We argue that the Mn magnetic order induces the spin polarization at high temperature. We interpret the kink in the integrated intensity as the onset of the noncollinear magnetic phase, which involves also the ordering of the 4*f* moment. This leads to an additional spin polarization of the 5*d* states due to the 4*f*-5*d* exchange. Thus, XRES as an element and band specific probe reveals a spin polarization in the Tb 5*d* states induced by the long range order of Mn, an effect that cannot be observed with neutron diffraction. For an insulator, such a coupling has not yet been observed. This indicates a strong hybridization between Mn and Tb, which we consider as a prerequisite for the occurrence of a modulated chiral phase at $T_{N'}$ and, thus, for ferroelectricity.

## ACKNOWLEDGMENTS

The authors gratefully acknowledge valuable discussions with S. Picozzi and S. Blügel. Use of the Advanced Photon Source was supported by the U.S. Department of Energy, Basic Energy Sciences, Office of Science, under Contract No. W-31-109-Eng-38. The MUCAT sector at the APS is supported by the Department of Energy, Office of Science, through the Ames Laboratory Contract No. W-7405-Eng-82.

[1] M. Fiebig, J. Phys. D **38**, R123 (2005).
[2] T. Kimura, T. Goto, H. Shintani, K. Ishizaka, T. Arima, and Y. Tokura, Nature (London) **426**, 55 (2003).
[3] T. Kimura, G. Lawes, T. Goto, Y. Tokura, and A. P. Ramirez, Phys. Rev. B **71**, 224425 (2005).
[4] N. Hur, S. Park, P. A. Sharma, J. S. Ahn, S. Guha, and S. W. Cheong, Nature (London) **429**, 392 (2004).
[5] S. Quezel, F. Tcheou, J. Rossamignod, G. Quezel, and E. Roudaut, Physica B & C **86**, 916 (1977).
[6] R. Kajimoto, H. Yoshizawa, H. Shintani, T. Kimura, and Y. Tokura, Phys. Rev. B **70**, 012401 (2004).
[7] M. Kenzelmann, A. B. Harris, S. Jonas, C. Broholm, J. Schefer, S. B. Kim, C. L. Zhang, S. W. Cheong, O. P. Vajk, and J. W. Lynn, Phys. Rev. Lett. **95**, 087206 (2005).
[8] M. Mostovoy, Phys. Rev. Lett. **96**, 067601 (2006).
[9] I. A. Sergienko and E. Dagotto, Phys. Rev. B **73**, 094434 (2006).
[10] H. Katsura, N. Nagaosa, and A. V. Balatsky, Phys. Rev. Lett. **95**, 057205 (2005).
[11] M. Blume and Doon Gibbs, Phys. Rev. B **37**, 1779 (1988).
[12] J. P. Hill and D. F. McMorrow, Acta Crystallogr., Sect. A: Found. Crystallogr. **52**, 236 (1996).
[13] E. O. Wollan and W. C. Koehler, Phys. Rev. **100**, 545 (1955).
[14] A. Stunault, F. de Bergevin, D. Wermeille, C. Vettier, T. Brückel, N. Bernhoeft, G. J. McIntyre, and J. Y. Henry, Phys. Rev. B **60**, 10170 (1999).
[15] J. Strempfer *et al.* (unpublished).
[16] S. C. Perry, M. M. R. Costa, W. G. Stirling, M. J. Longfield, D. Mannix, and T. Brückel, J. Phys.: Condens. Matter **10**, 1951

(1998).

[17] S. Langridge, J. A. Paixao, N. Bernhoeft, C. Vettier, G. H. Lander, D. Gibbs, S. A. Sorensen, A. Stunault, D. Wermeille, and E. Talik, Phys. Rev. Lett. **82**, 2187 (1999).

[18] O. Prokhnenko, R. Feyerherm, E. Dudzik, S. Landsgesell, N. Aliouane, L. C. Chapon, and D. N. Argyriou, Phys. Rev. Lett. **98**, 057206 (2007).

[19] J. S. Smart, *Effective Field Theories of Magnetism, Studies in Physics and Chemistry* (Saunders, Philadelphia, 1966).

[20] J. P. Perdew, K. Burke, and M. Ernzerhof, Phys. Rev. Lett. **77**, 3865 (1996).

[21] S. Picozzi, K. Yamauchi, G. Bihlmayer, and S. Blügel, Phys. Rev. B **74**, 094402 (2006).